



HAL
open science

Addressing the ill-posedness of multi-layer porous media characterization in impedance tubes through the addition of air gaps behind the sample: numerical validation

Rémi Roncen, Zine El Abiddine Fellah, E Ogam

► To cite this version:

Rémi Roncen, Zine El Abiddine Fellah, E Ogam. Addressing the ill-posedness of multi-layer porous media characterization in impedance tubes through the addition of air gaps behind the sample: numerical validation. *Journal of Sound and Vibration*, 2022, 520, pp.116601. hal-03410907v2

HAL Id: hal-03410907

<https://hal.science/hal-03410907v2>

Submitted on 1 Nov 2021

HAL is a multi-disciplinary open access archive for the deposit and dissemination of scientific research documents, whether they are published or not. The documents may come from teaching and research institutions in France or abroad, or from public or private research centers.

L'archive ouverte pluridisciplinaire **HAL**, est destinée au dépôt et à la diffusion de documents scientifiques de niveau recherche, publiés ou non, émanant des établissements d'enseignement et de recherche français ou étrangers, des laboratoires publics ou privés.



Distributed under a Creative Commons Attribution - NonCommercial - NoDerivatives 4.0 International License

Addressing the ill-posedness of multi-layer porous media characterization in impedance tubes through the addition of air gaps behind the sample: numerical validation

R. Roncen ^{*1}, Z.E.A. Fellah ^{†2} and E. Ogam ^{‡2}

¹ONERA /Département Multi-Physique pour l'Énergétique, Université de Toulouse, F-31055, Toulouse, France

²Laboratoire de Mécanique et d'Acoustique, Centre National de la Recherche Scientifique, Unité Mixte de Recherche 7031, Aix-Marseille Université, Centrale Marseille, F-13402 Marseille Cedex 20, France

Abstract

This paper is concerned with plane wave propagation in multi-layer assemblies of rigid isotropic porous media inside impedance tubes. The focus is placed on the inverse problem, i.e., the retrieval of the intrinsic properties defining the pore micro-structure of each layer: the porosity, the pore mean size and the pore size standard deviation. Each layer is considered isotropic. Such an inverse problem can be ill-posed due to the non-uniqueness of the solution. The technique explored in this work is the consideration of additional acoustic observations, where air gaps are placed behind the multi-layer assembly. The aptitude of this strategy to overcome the ill-posedness of the inverse problem is evaluated on numerical synthetic data, on assemblies made of three layers. For a given fixed amount of input data, inverse problems including different observations with air gaps can yield more accurate results, removing the

*remi.roncen@onera.fr

†fellah@lma.cnrs-mrs.fr

‡ogam@lma.cnrs-mrs.fr

ill-posedness.

Key-words: impedance tube; porous materials; material characterization; Bayesian inference; multi-layer materials; air gaps

1 Introduction

A porous material can be represented as the combination of a solid phase and a fluid phase. Interactions and energy exchanges occurring between the two phases give rise to the dissipation of waves traveling through the porous medium. In air-saturated porous media, wave dissipation is mostly caused by visco-inertial and thermal effects which strongly depend on the pore microstructure [1]. To represent this geometry at the macroscopic scale, several intrinsic porous material properties (i.e., porosity, tortuosity, pore size, etc.) have been derived and integrated in models governing the acoustic wave behavior.

These intrinsic properties are of interest in a wide range of applications outside of the acoustic domain, because porous media are largely present in our environment and are used in various fields: in geophysics [2] for the detection of seismic waves [3, 4] or for the detection of land mines [5, 6]; in medicine for the study of bones [7–9]; in aeronautics for the reduction of trailing edge noise [10–12]; in thermal engineering, for transpiration-cooling in combustion chambers [13, 14]; in room acoustics, with sound absorbing foam [15, 16]. A shared feature of these research topics is that the knowledge of the intrinsic properties of porous materials is needed for the use of predictive models (i.e., wave propagation in soil for seismic applications, risk fracture assessment for porous bone, acoustic absorption for foams).

The measurement of each individual intrinsic property of a porous material is a difficult task, often requiring multiple independent experiments [17–20]. As a result, different indirect measurement approaches have been developed, based on the resolution of an acoustic inverse problem [21, 22]. Having measured an acoustic field that has interacted with a given porous material, and given a model that can represent well the acoustic behavior of said porous material as a function of its

intrinsic properties, the goal becomes that of finding the parameters of the numerical model that allow to best match the experimental data. It is then assumed that the numerically inferred values for the parameters of interest are the “true” values.

This paper is concerned with such an inverse problem, for the case where rigid multi-layer materials are considered. The mechanical behavior of the frame, and the potential coupling between fluid and solid phase, are not considered in this work. Furthermore, each layer is assumed to be isotropic, so that 1D wave propagation can be considered.

The inverse problem of single-layer material identification has been thoroughly studied in different frequency regimes, with various acoustic models and experimental setups [21, 22]. However, there is little in the literature about the identification of multi-layer materials with acoustic inverse methods, i.e., finding simultaneously the intrinsic properties of two or more than two materials that are stacked on one another [23–25]. When dealing with a fixed number of known materials that can be characterized independently, there is no need for such a multi-layer identification. However, when a single material is inhomogeneous and can be approximated by a discrete number of unknown isotropic layers, the method becomes relevant [23].

The contribution of de Ryck et al. [23] established a method for the identification of porous materials having inhomogeneous profiles of material properties (i.e., the porosity, tortuosity, etc.). Using a conjugate gradient algorithm and a deterministic approach for the minimization of the reflection coefficient, they were able to reconstruct complex property profiles from synthetic numerical data (with and without noise). However, when more than one property was identified at a time, the reconstruction was degraded, even in the noiseless case where no Gaussian noise is added to pollute the signals. The work of Fellah et al. [24] was concerned with the inverse problem for the identification of two layers of rigid porous media, using reflected waves in the ultrasonic range as input for their deterministic inverse method. Using a smaller subset of model parameters that were shown to be sensitive with respect to the reflection coefficient, the inverse problem was shown to be well-posed and to admit a unique solution. A recent contribution by Fackler et al. [25] has

attempted the analysis of the inverse problem for multi-layer materials, using two levels of Bayesian inference (parameter identification and model selection), showing that it was possible to not only detect the number of layers in a material, but also identify some of their properties, and the associated uncertainties. However, as in previous studies on porous media identification [26–28], ill-posedness was present in the identification, i.e., there was a non-uniqueness, an indetermination of the obtained parameters of interest. Bayesian inference methods are well suited for this kind of difficult task, in that they yield posterior probability densities for the parameters of interest containing all the knowledge one is able to extract from the signals. Thus, the non-uniqueness of the solution can be characterized, provided that the Bayesian inference sufficiently explored the parameter space. It then becomes possible to quantify the effectiveness of new methods attempting to remove part of the inverse problem ill-posedness.

There seems to be three important practical choices that one must make before solving an inverse problem for the identification of porous media properties, depending on the type of available acoustic measurement:

- The frequency content of the signal (low-mid frequency range in wave guides [22, 25–27, 29–32], or high frequency range with ultrasonic transducers in free space [28, 29, 33–39]).
- The nature of the inverse problem (deterministic when an optimization approach is used [29–36], or statistic when a Bayesian inference is used [25–28, 32, 37–39]).
- The type of signal (time-domain [27, 28, 33–38] or frequency-domain [25, 26, 29–32, 39]).

In our previous studies, we were interested in solving the inverse problem (using a Bayesian approach) on air-saturated isotropic rigid porous materials (plastic foam) using the equivalent fluid model [37, 38] and on water-saturated porous materials (bone tissue and biomaterials) using the Biot model [28, 40]. The high-frequency regime was studied using experimental ultrasound data [28, 37, 38, 40]. The low frequency regime was also studied for air-saturated porous materials [27]. Since we were measuring transient signals, the time-domain signals were used to “feed” the inference process. In the present work, frequency-domain signals at low-mid frequencies are used.

This choice is driven by the actual set-up in which, ultimately, experiments would be performed (i.e., the impedance tube, where frequencies ranging from 200 Hz to 5.5 kHz can be observed). Signals acquired in impedance tubes are typically treated in the frequency domain. Finally, Bayesian inference is chosen since it allows for an improved characterization regarding the ill-posedness of the problem [25, 26, 28].

The first objective of this paper is to evaluate the merit of a technique based on the addition of air gaps behind the samples to reduce the ill-posedness and improve the knowledge on material properties of both single- and multi-layer samples. Although air gaps are traditionally used to improve the acoustic absorption of sound-absorbing foams in the low-frequency range [41], they are used in the present work to gain additional observations of the same samples for parameter identification purposes, in an attempt to over determine the inverse problem. This was tried previously by Sellen et al. [42], albeit with additional boundary conditions at the end of the impedance tube. A similar strategy was also attempted by Zieliński et al. [31] for the deterministic identification of the Jonhson-Champoux-Allard-Lafarge (JCAL) model parameters of single-layer materials, making use of surface impedance measurements and two scaling factors to obtain a set of normalized dimensionless parameters. Air gaps of known thicknesses were used, but without quantifying their benefit to the identification procedure.

The present study merges elements of the works of Refs. [25, 31], showing a straightforward strategy for the removal of ill-posedness in the inverse problem for multi-layer material identification. The influence of additional air gaps in porous media identification is exposed, using Bayesian inference to highlight cases of non-uniqueness in the inverse problem. In addition, it is shown that using surface impedances or reflection coefficients obtained from impedance tubes as the input for the inverse characterization is bound to yield biased identification results, because of frequency-dependent uncertainties not being correctly taken into account.

The paper is organized as follows. The acoustical model and methods applied to a porous material are first summarized in Sec. 2. A source of bias in the inverse characterization based on impedance tube measurements is highlighted in Sec. 3. The Bayesian inference framework is given

in Sec. 4. Section 5 presents and discusses the identification results obtained on different *numerical* tests with synthetic noisy data, and Sec. 6 summarizes the takeaway messages and concludes the paper.

2 Acoustical model

The porous material samples considered in this work are assumed to have a rigid structure. Porous samples thus behave as an equivalent fluid when considering the dissipation of an acoustic wave traveling within the intra-pore fluid phase (air). Visco-inertial effects are introduced in the definition of a complex frequency-dependent density $\tilde{\rho}_{\text{eq}}$, whereas thermal effects and stiffness of the medium are introduced in the definition of a complex frequency-dependent bulk modulus \tilde{K}_{eq} . The equation controlling the wave behavior inside the fluid phase is written

$$\Delta p + \omega^2 \frac{\tilde{\rho}_{\text{eq}}}{\tilde{K}_{\text{eq}}} p = 0. \quad (1)$$

Wave dissipation in the pores is accounted for, in the present work, by the Jonhson-Champoux-Allard-Pride-Lafarge (JCAPL) model [43–46] and the hypotheses on the pore distribution by Horoshenkov [47], i.e., the pore size distribution is assumed to follow a log-normal distribution and the pores have a circular shape. Using these hypotheses, it is possible to use only three parameters to fully define $\tilde{\rho}_{\text{eq}}$ and \tilde{K}_{eq} , namely the porosity ϕ , mean pore size \bar{s} and pore size standard deviation σ_s (normalized by $\log(\bar{s})$) [47].

The main reason for the choice of using the Horoshenkov hypotheses is the simplicity of the model: having fewer parameters can greatly reduce the complexity of an inverse problem. Because of the wide variety of areas of application for the inverse characterization of the intrinsic properties of porous media, it also seems valuable to use a model whose properties (pore size and standard deviation) have a straightforward meaning to the end user, while some of the JCAPL model properties are defined in the high and low frequency limits with integrals of the velocity profile within the pores. The Horoshenkov hypothesis on the log-normality of the pore size distribution covers a large range of porous materials (fibrous, granular, foam), and has been favorably compared

to surface impedance data obtained in impedance tubes [47]. The choice in this work to use the JCAPL model as the basis for the Horoshenkov hypothesis is motivated by the widespread use of the JCAPL model in the acoustic community, and the straightforward changes required to apply the hypothesis allowing the reduction in the number of parameters required. The JCAPL-Horoshenkov model is also well adapted to impedance tube measurements, typically performed in the medium frequency range, since it connects the high-frequency and low-frequency limits.

The approach followed in this work does not impose the use of a specific model for the identification, and could be straightforwardly attempted with a different pore dissipation model.

3 A source of bias in material characterization

In this section, the synthetic model for wave propagation in an impedance tube is first recalled (see Sec. 3.1). It is then shown why using the surface impedance or reflection coefficient in the inverse characterization of a porous material might lead to biased results, due to the uncertainty being a nonlinear function of the frequency (see Sec. 3.2).

3.1 Wave propagation in a model impedance tube

An impedance tube is a device made up of a loudspeaker connected to a tube, ending with a rigid backing. Porous materials are placed at the end of the tube, and microphones are located along the tube. In practice, the goal is to use the pressure measurements to separate the incident and reflected waves from the standing wave pattern created within the tube. A schematic of the tube is shown in Fig. 1. In this paper, only numerical synthetic data is considered. However, the dimensions, frequency bands and material properties were chosen to be representative of typical impedance tube measurements in our lab. In the following, the notion of “measurement” always refer to the numerical extraction of a value from our code. The pressure at the microphone locations x_i can then be numerically evaluated, provided that both the source coefficient \tilde{A} of the loudspeaker and the reflection coefficients are known. The acoustic pressure p inside the impedance tube is, for

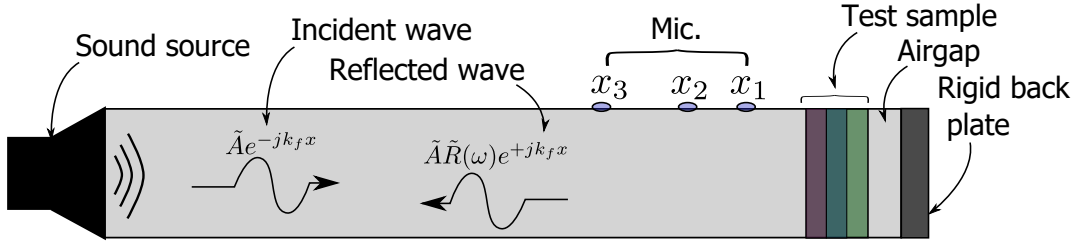


Figure 1: Schematics of an impedance tube

plane waves,

$$p(x, \omega) = \tilde{A}e^{-jk(\omega)x} + \tilde{A}\tilde{R}(\omega)e^{+jk(\omega)x}, \quad (2)$$

with the source coefficient \tilde{A} , \tilde{R} the normal incidence reflection coefficient of the porous sample, j the imaginary unit, x the longitudinal microphone locations in the tube and where $k(\omega) = \omega/c_f$ is the propagation wavenumber of air for the plane wave (here the tube is assumed wide enough to neglect viscous effects at the walls), with c_f the speed of sound.

The reflection coefficient is obtained by the solving of the linear system

$$\begin{bmatrix} p_1 \\ p_2 \\ p_3 \end{bmatrix} = \begin{bmatrix} e^{-jk(\omega)x_1} & e^{+jk(\omega)x_1} \\ e^{-jk(\omega)x_2} & e^{+jk(\omega)x_2} \\ e^{-jk(\omega)x_3} & e^{+jk(\omega)x_3} \end{bmatrix} \cdot Q, \quad (3)$$

with $Q = [\tilde{A}, \tilde{R}]^t$ and where the notation $p_i = p(x_i, \omega)$ is used.

Note that this approach is not always followed. It is sometimes found in the literature that pressure measurements are used in pairs to identify the reflection coefficient, the pair being selected only at certain frequencies related to the spacing between the microphones [48]. Although this is justified when only two microphones are available, it is argued here that using all microphones simultaneously (instead of two at a time) is strictly better, since the information content is increased. For the proper placement of microphones, guidelines are provided in Ref [48].

3.2 Evaluating the uncertainty on the reflection coefficient

Using the transfer matrix method of Ref. [1, Chap. 11], the total reflection coefficient $\tilde{R}(\omega)$ can be calculated at normal incidence for a sample, with or without an air gap. The degree of uncertainty

of the pressure measurements is usually a complex function of the frequency, because of different biases (imprecision in the mounting of microphone, imprecision in the exact location of the upper surface of the porous sample). Here, for simplicity, it is modeled by a zero-mean Gaussian noise of constant standard deviation across all frequencies.

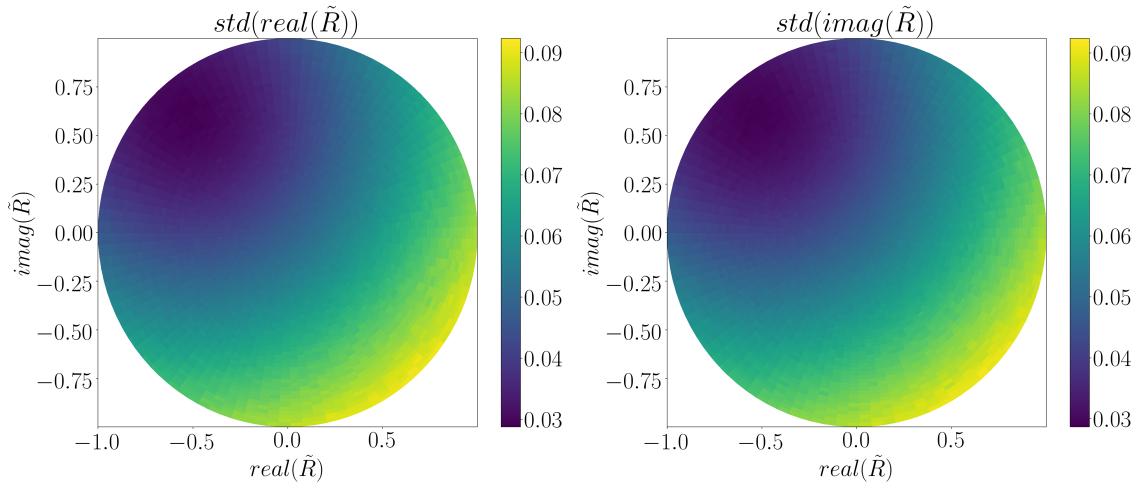
Numerical experiment: A fixed uncertainty on the real and imaginary parts of microphone pressure measurements is considered for a given reflection coefficient. We are interested in what becomes of this uncertainty when propagated in the calculated reflection coefficient. The following steps are performed successively at each frequency of interest:

- Select a value of the reflection coefficient $\left\{ \tilde{R}(\omega) \in \mathbb{C}, \left| \tilde{R}(\omega) \right| \leq 1 \right\}$, fix $\tilde{A} = 1$.
- Calculate the pressure p_i , $i = 1, 2, 3$ at the three microphone locations x_i , $i = 1, 2, 3$ using Eq. 2. The distance between microphones i and k is noted $d_{i,k}$: $d_{1,2} = 10$ mm, $d_{2,3} = 70$ mm.
- Add a random Gaussian noise to the three numerical pressures (i.e., synthetic signals mimicking the measurements), with standard deviation $\sigma = 0.05$ on both the real and imaginary parts, i.e.,

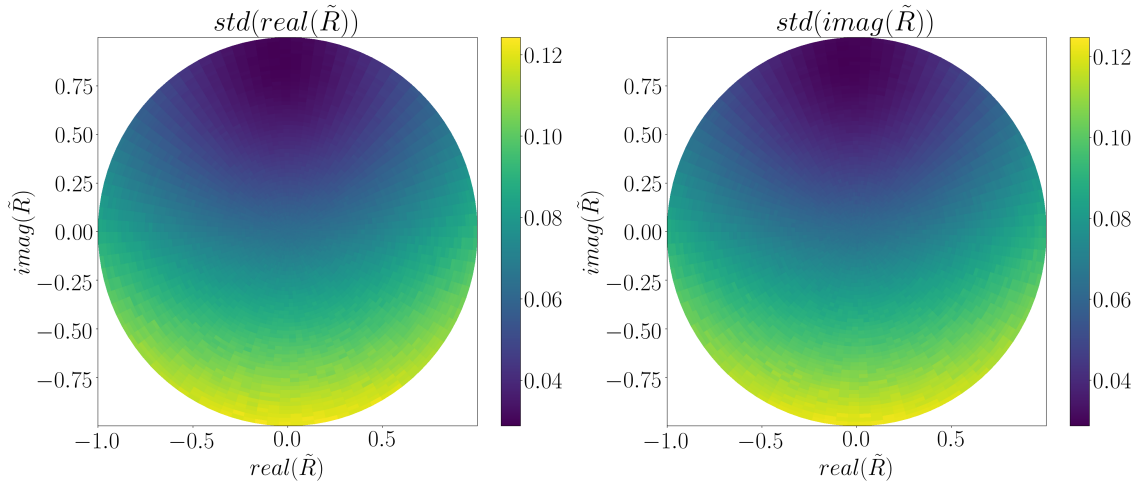
$$- \epsilon_{R,i} \sim \mathcal{N}(0, \sigma), \quad \epsilon_{I,i} \sim \mathcal{N}(0, \sigma) \implies p(x_i) = p(x_i) + \epsilon_{R,i} + j\epsilon_{I,i}, \quad i = 1, 2, 3.$$

- Obtain the reflection coefficient from the noisy pressure measurements using Eq. 3.

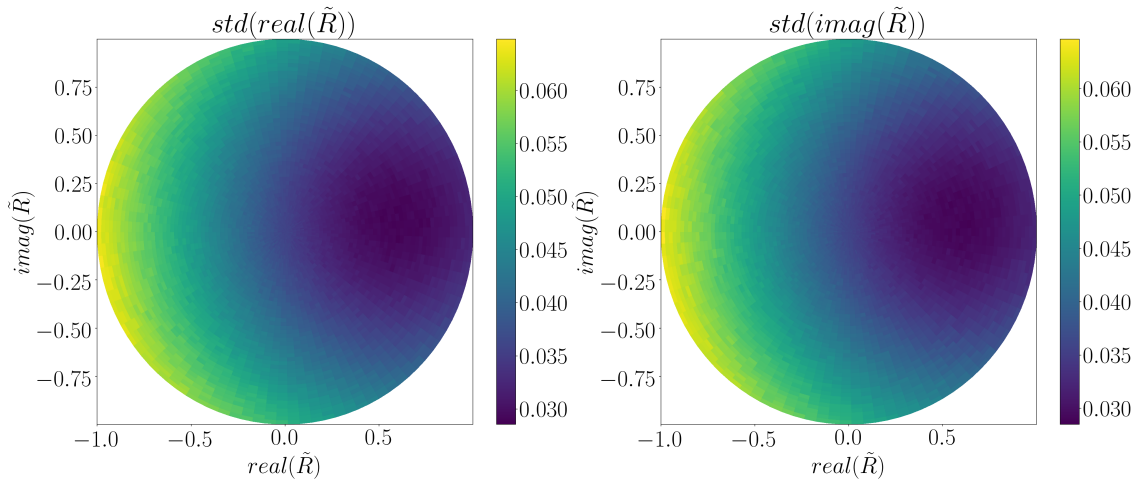
The previous steps are repeated 10^4 times at each frequency for each value of the reflection coefficient, to provide converged statistics. The quantity of interest here is the standard deviation of the error on both the real and imaginary parts of the reflection coefficient, calculated from the noisy signals. These are shown for some frequencies of interest in Fig. 2.



(a) 500 Hz.



(b) 2000 Hz.



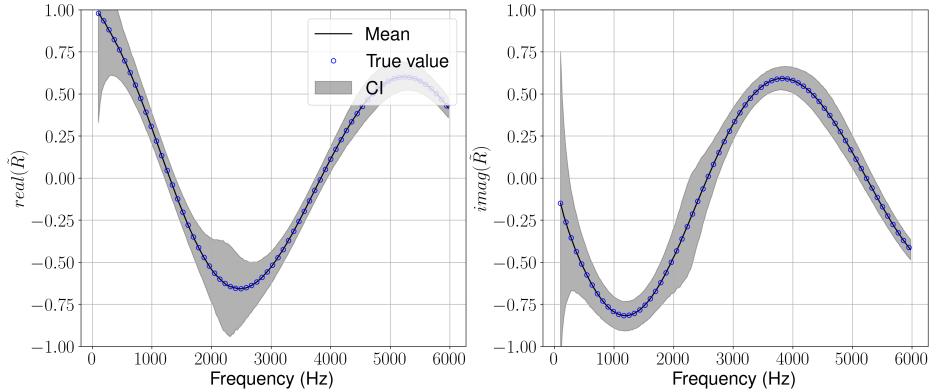
(c) 4000 Hz.

Figure 2: Standard deviation of the real (left) and imaginary (right) parts of the reflection coefficient.

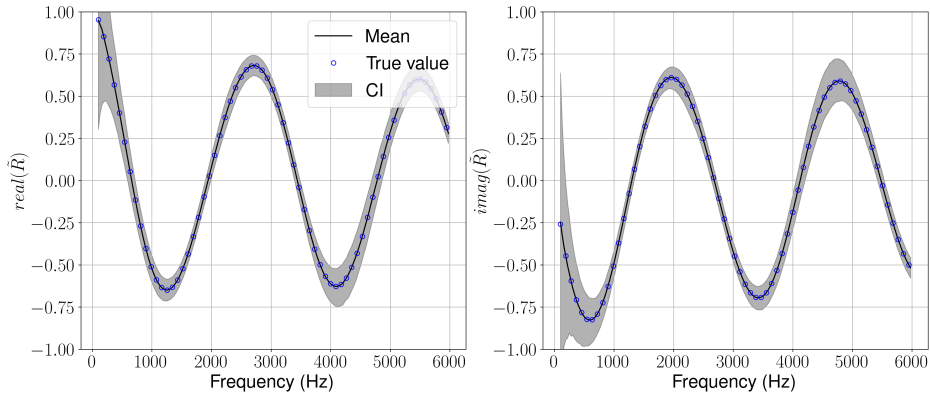
The standard deviations of the real and imaginary parts display a similar trend at a given frequency. However, the uncertainty on the reflection coefficient is clearly frequency dependent, and depends on the reflection coefficient value as well. This makes any inference approach based on the reflection coefficient an unnecessarily complex process, since one would first have to estimate a value of the uncertainty at each frequency, for each value of the reflection coefficient. If this is not done, and one takes an average uncertainty, then a bias is present in the identification, by giving more weight to frequencies with high uncertainties, and less weight to frequencies with low uncertainties. The same could be said about the impedance and the absorption coefficient, even more so with the impedance since its values are not bounded, thus creating even larger contrasts of uncertainties depending on the frequency and impedance value.

To prove the previous points, a numerical test is performed where the reflection coefficient and associated uncertainties are given in Fig. 3 for a single-layer porous material, whose acoustic behavior is governed by the model detailed in Sec. 2. Material properties are $\phi = 0.98$, $\bar{s} = 250 \mu\text{m}$ and $\sigma_s = 0.05$, which are properties close to those of typical rigid acoustic foams. Two cases are considered, one with no air gap, and one where an air gap of 30 mm is placed between the material and the rigid backing plate of the impedance tube.

In both cases, the mean value of the 10^4 runs perfectly matches the true value, on the whole frequency spectrum. The uncertainty is important in both cases at low frequencies. This is caused by the maximum microphone spacing (80 mm) and the linear system 3 becoming increasingly more ill-conditioned, resulting in some cases in $|\tilde{R}(\omega)| > 1$. At around 2000 Hz, the uncertainty becomes large again only for the reference reflection coefficient with no air gap present. Note that the error distribution does not necessarily always follow a normal distribution, because the mapping having the pressure signals as input and the reflection coefficient as output is not linear. This is seen in Fig. 3 by the slight lack of symmetry, at certain frequencies, of the credibility intervals (CI) around the mean value. The main consequence of this test is that adding an air gap may allow the experimenter to better observe parts of the signals, because of the uncertainty distribution in the observation with an additional air gap being different from that in the reference no air gap observation. Said differently, a frequency band can be shadowed in one experiment because of high



(a) Without an air gap



(b) With an air gap of 30 mm placed behind the material

Figure 3: Real and imaginary parts of the reflection coefficient of a foam of thickness 30 mm with a porosity of $\phi = 0.98$, a mean pore size $\bar{s} = 250 \mu\text{m}$ and a pore size standard deviation of $\sigma_s = 0.05$. The gray areas correspond to the limits containing $\approx 95\%$ of the 10^4 samples that were used to obtain converged statistics. The symbols correspond to the exact values that were used in generating the numerical pressures.

uncertainties, and display small uncertainties when an air gap has been added. This is caused by an air gap changing the real and imaginary part of the reflection coefficient, which has a direct impact on the uncertainty, as shown in Fig. 2.

4 Bayesian inference for inverse identification of porous material properties

Given relevant observations (here, numerically generated acoustic pressures), one can use Bayes' theorem to update one's knowledge and draw conclusions about certain hypotheses. One of the tenets of the Bayesian approach to statistics is to interpret knowledge, or degree of belief, as a

quantity represented by probabilities [49, Chap. 8].

This section presents the different elements required to perform the Bayesian inference of the model parameters of interest. The Bayesian inference approach used to find the posterior density functions of the parameters is recalled, as well as the specific numerical strategy.

In Bayesian inference, knowledge of a parameter is represented by its probability density function (pdf). Bayes theorem on conditional probabilities writes

$$P(\theta|\mathcal{D}, I) \propto P(\mathcal{D}|\theta) P(\theta, I), \quad (4)$$

where θ represents the model parameters to identify, \mathcal{D} represents the observed data (real and imaginary parts of the pressure), and I represents background general information, such as the choice of model (for the porous wave propagation and for the noise on the observed data). The goal is to sample from $P(\theta|\mathcal{D}, I)$, the *posterior* probability, to reconstitute the pdf of each parameter. The *likelihood* $P(\mathcal{D}, I|\theta) = \mathcal{L}(\theta)$ represents the goodness of fit between the data and the model, for given values of model parameters. Since a Gaussian hypothesis is made regarding the error on the pressure measurements (assumed distinct and independent for the real and imaginary parts of the signals, but constant across the microphones), one can write the likelihood as the product of likelihoods for the real and imaginary parts of the observations:

$$\mathcal{L}(\theta) = (2\pi\sigma_R)^{-N/2} e^{-\frac{S_R}{2\sigma_R^2}} \times (2\pi\sigma_I)^{-N/2} e^{-\frac{S_I}{2\sigma_I^2}}, \quad (5)$$

$$S_R = \sum_{m=1}^{N_{\text{exp}}} \sum_{k=1}^{N_{\text{micro}}} \sum_{n=1}^{N_{\text{freq}}} \text{real}(p_{m,k,n}^{\text{obs}} - p_{m,k,n}^{\text{num}})^2, \quad S_I = \sum_{m=1}^{N_{\text{exp}}} \sum_{k=1}^{N_{\text{micro}}} \sum_{n=1}^{N_{\text{freq}}} \text{imag}(p_{m,k,n}^{\text{obs}} - p_{m,k,n}^{\text{num}})^2, \quad (6)$$

where N is the number of observed data points ($N = N_{\text{exp}} \times N_{\text{freq}} \times N_{\text{micro}}$), with N_{exp} the number of numerical ‘‘experiments’’ ($N_{\text{exp}} = 1$ in the reference case where no air gap has been added, and $N_{\text{exp}} = 1 + N_{\text{airgap}}$ when air gaps have been added). N_{freq} is the number of frequencies contained in a signal and N_{micro} the number of microphones (here 3). The error standard deviations of the real and imaginary parts of the pressure measurements are denoted σ_R and σ_I , respectively. In the case of the present numerical study, the exact synthetic signals are polluted with the addition

of a Gaussian noise on their real and imaginary parts. This is a rather strong hypothesis, made to simplify the analysis, as we ignore non-Gaussian biases that are present in actual experiments (i.e., microphone mounting, imprecision on the material placement relative to the microphones). Finally, $p_{k,n}^{\text{obs}}$ is the observed pressure signal (with a zero-mean Gaussian noise added to it) at the k^{th} microphone and n^{th} frequency, whereas $p_{k,n}^{\text{num}}$ is the numerical pressure evaluated with Eq. 2 after the reflection coefficient $\tilde{R}(\omega)$ was calculated using the transfer matrix approach, with parameters θ as input. Note that in practice, the logarithm of the likelihood is used to avoid numerical zeros.

The *prior* probability $P(\theta, I)$ represents all the information one may have on the parameters before the new observation. For instance, one might have a precise measurement of the thickness of a sample, or an air gap, and use the prior probability to encode this knowledge by a normal law of low standard deviation on the thickness parameter. Bayesian inference would then favor solutions respecting this added knowledge. In the present work, however, it was decided to not consider strong previous knowledge, to conduct a blind inference where only the acoustic data would drive the parameter inversion. The parameter space is made of the Horoshenkov model parameters of each porous sample, their thickness $L_{p,i}$, the temperature T and static pressure P_0 (used to calculate air properties, assuming an ideal gas law), the standard deviations σ_R and σ_I of the real and imaginary parts on the microphone pressure signals, and the length of the air gaps $L_{a,j}$, if any. Uniform probabilities of broad supports are used for the prior to represent an initially uninformative state of knowledge, whose bounds are given in Table 1. The only exception is for the static pressure, for which a smaller relative prior support is chosen when multi-layer materials are considered. This is done because it is the only parameter that was shown to have close to zero influence on the identification. Single-layer materials were considered first in this study, and their support for P_0 was $[0.8 - 1.2 \cdot 10^5] Pa$.

Overall, Eq. 4 represents how the prior knowledge on the parameters is updated by the observation of new data \mathcal{D} , under certain hypotheses I . Only the first level of Bayesian inference is conducted, i.e., that of parameter identification. To obtain the posterior pdf of each parameter, a numerical approximation is obtained by the use of a Markov Chain Monte Carlo algorithm (MCMC).

Table 1: Prior bounds of the parameters, where the symbol – means that there is no unit. The indices i and j denote the layer number and air gap number, respectively.

Parameter	σ_R	σ_I	T	P_0	$L_{p,i}$	ϕ_i	\bar{s}_i	$\sigma_{s,i}$	$L_{a,j}$
Unit	Pa	Pa	°C	10^5 Pa	mm	–	μm	–	mm
Min	10^{-4}	10^{-4}	5	0.95	5	0.1	10	0	1
Max	0.5	0.5	25	1.05	40	0.999	10^3	0.99	100

The chosen MCMC approach is the Multiple-Try DiFFeRential Evolution Adaptive Metropolis with sampling from past State: MT_DREAM (ZS) [50–52], because it was shown to work even in the case of multi-modal distributions (at least up to a dimension of 25 [52, Sec. 3.2] for a tri-modal Gaussian distribution with well separated modes), and was used in our earlier works in porous media identification [27, 28, 37, 38, 40]. The ability to capture multi-modality is required to evaluate the inverse problem ill-posedness (in the sense of non-uniqueness of the solution). To check the convergence of the chains, a Gelman-Rubin criterion was used [53] a posteriori, after a fixed set of $3 \cdot 10^5$ iterations. In practice, this number of iterations should be as large as possible, given one’s numerical budget. The number of iterations required to reach a given value of the Gelman-Rubin criterion (typically, under 1.05) is case-dependent and would highly vary if another model were to be used for the equivalent fluid. In the present study, inferences on single-layer materials could reach convergence in as little as $5 \cdot 10^4$ iterations, while some triple-layer materials never did, due to the inability of the criterion to handle multi-modal distributions. In these cases, a visual check was done on each chain individually to ensure their proper mixing. The MCMC python code implementation that was used is freely available under the GNU GPLv3 license at <https://github.com/LoLab-VU/PyDREAM>, and was created by the Lopez Lab at Vanderbilt University [54]. Three chains were used in parallel, and the number of multi-try was set to 5.

Once the Markov chains have converged, one can take different estimates to evaluate the porous media parameters. A common choice is to extract the set of parameters that maximize the left term of Eq. 4, also known as maximum a posteriori (MAP), and retrieve credibility intervals. The interested reader is referred to Ref. [49, Chap. 8] for a more general introduction to Bayesian estimates, and to Refs. [27, 28] for applications on porous media. In the present study, it was

elected not to give any particular estimate, as the main purpose of this work is to assess the influence of a method on the inverse problem ill-posedness. A graphical display of the pdf allows one to check the ill-posedness in a straightforward manner via the existence of multiple modes.

5 Results

5.1 Description of the numerical tests

Three numerical materials were used, M_1 , M_2 and M_3 , whose properties are summarized in Table 2. In practice, here are the steps followed for the numerical study:

Table 2: Properties of the model for materials M_1 , M_2 , M_3

Model properties [47]			
Material	ϕ	\bar{s} (μm)	σ_s
M_1	0.85	100	0.2
M_2	0.65	50	0.5
M_3	0.98	250	0.05

- A single or multi-layer material is chosen, with or without an air gap, and the numerical reflection coefficient is calculated by the transfer matrix approach.
- The *numerical* synthetic pressure signals are evaluated at $x_1 = 2$ cm, $x_2 = 3$ cm and $x_3 = 10$ cm (with $x = 0$ at the material upper surface) with Eq. 2 and fixing the source coefficient at $\tilde{A} = 1$.
- A Gaussian noise is added to the pressure signals to represent the uncertainty, with $\sigma_R = 0.05$ and $\sigma_I = 0.08$ the standard deviations of the error on the real and imaginary parts of the signals, respectively. See Fig. 4 for a representation of these signals for material M_1 of thickness $L_1 = 30$ mm, without an air gap.

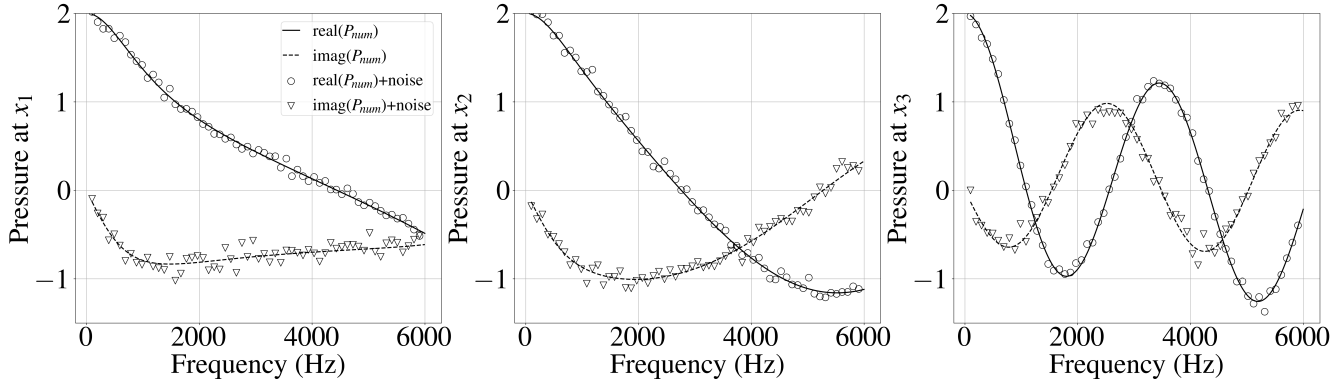


Figure 4: Microphone signals (exact and with added zero-mean Gaussian noise) in the impedance tube for material M_1 at the fictive microphone locations.

- The noisy pressure signals are then used as input to Bayesian inference process, mimicking what the experimenter would do with experimentally obtained impedance tube measurements.

The reader familiar with inverse problems will have noticed that in the current numerical analysis, the same model is used to generate the synthetic data and to infer the model parameters. This is sometimes referred to as an inverse crime [55], because of the more manageable aspect of the inverse problem in such cases (thus potentially hiding the true difficulty of the same approach on real experimental data). There is a practical interest in using an inverse crime, when trying to explore new methods [55]. The focus of this paper is placed on the evaluation of ill-posedness in the inverse identification of multi-layer porous media parameters. To ease the analysis and compare the reference method (without an air gap) to the one developed in this work, it is convenient to know in advance the true model parameter values, hence the use of a similar model for both the direct and inverse problems [23, 31].

The addition of a Gaussian noise to pollute the signals can, counter-intuitively, make the problem more tractable. Without noise, the likelihood has a very steep gradient near the true value of the parameters, which can make the exploration of the posterior densities more challenging for some MCMC strategies, and increase the occurrence of multi-modal distributions (the equivalent of local minima when using a standard optimization approach to an inverse problem). It was chosen to add a noise with a standard deviation between 5 – 8% of the input signal amplitude

$\tilde{A} = 1$ of the source wave ($\sigma_R = 0.05$ and $\sigma_I = 0.08$). This is equivalent to having a standard deviation of about 0.5 dB in the pressure signals, for an incident wave amplitude of 94 dB.

5.2 Sample configurations

A summary of the sample combinations that are identified is given in Table 3.

Table 3: Summary of the 6 sample configurations. The symbol \circ means the stacking of materials, with the left term being the one closest to the acoustic source.

One layer	Three layers
Combination	Combination
M_1	$M_1 \circ M_2 \circ M_3$
M_2	$M_2 \circ M_1 \circ M_3$
M_2	$M_3 \circ M_2 \circ M_1$

First, the Bayesian inference identification process is performed on each sample (whose thickness is fixed at 30 mm) individually, with or without air gaps. This makes it possible to show how the method performs in a default situation with only one layer to identify. The identification of multi-layers made up of three single layers is then performed. The total thickness of the multi-layer is always taken to be 30 mm (not including air gap), distributed equally on all layers. For each sample configuration, 2 different inferences are conducted (Case 1 and Case 2), where the number of air gaps and the number of frequencies in a signal are varied. The cases are summarized in Table 4. In Case 1, a single observation is performed, and the pressure signals at the three microphone locations are recorded from 200 Hz to 6000 Hz, with a step in the frequency resulting in 4800 data points ($N_{\text{freq}} = 4800$ and the number of numerical “experiment” is $N_{\text{exp}} = 1$). In Case 2, the reference “no air gap” observation is also performed, and three additional observations are done with various air gaps. The pressure signals for all $N_{\text{exp}} = 4$ numerical experiments are recorded at the three microphone locations, from 200 Hz to 6000 Hz, with a frequency step resulting in $N_{\text{freq}} = 1200$ data points. As a result, the total number of data points $N = N_{\text{exp}} \times N_{\text{freq}} \times N_{\text{micro}}$ remains constant in both cases, but the frequencies considered are not the same (in practice, acquisition equipment has a fixed N_{freq}). The goal is to determine whether a change in the parameter identification

results is caused by the presence of air gaps in the observation, and not by an increase in the amount of observed data. In practice, however, one should take all the available information into consideration when performing the identification, and should not down sample the frequencies as done here for illustration purposes.

Table 4: Summary of the different observations used in each sample configuration. The \checkmark symbol means that the observation has been used for the inference. N_{freq} is the number of frequencies contained in a single signal, whereas N_{exp} is the number of numerical "experiment", corresponding to the number of ticks in a given line of this table.

Case	N_{freq}	No air gap	air gap length			$N_{\text{freq}} \times N_{\text{exp}}$
			2 cm	4 cm	6 cm	
1	4800	\checkmark				4800
2	1200	\checkmark	\checkmark	\checkmark	\checkmark	4800

In the following, the inference results of the 6 configurations of Table 3 are displayed. The pdfs are obtained by taking the samples of the MCMC chains, removing the first 20% samples as burn-in (so that the chains properly reach the density to explore), and using the seaborn [56] python package for the plot of the kernel density estimate.

5.3 single-layer identifications

The identifications of single layer materials are shown in Figs. 5,6,7 where the posterior pdfs all display a support that is sensibly smaller than the prior support in Table 1. While this is not a direct sign of convergence, it means that information was indeed gained from the observed signals. The closeness of all pdfs to the true value (vertical line in the figures) is a solid proof that the inverse problem is well resolved in all cases. Note that in Case 2, there are 3 additional parameters to identify (i.e., the air gap lengths), which makes the Bayesian inference strategy more complex and the parameter space more difficult to explore.

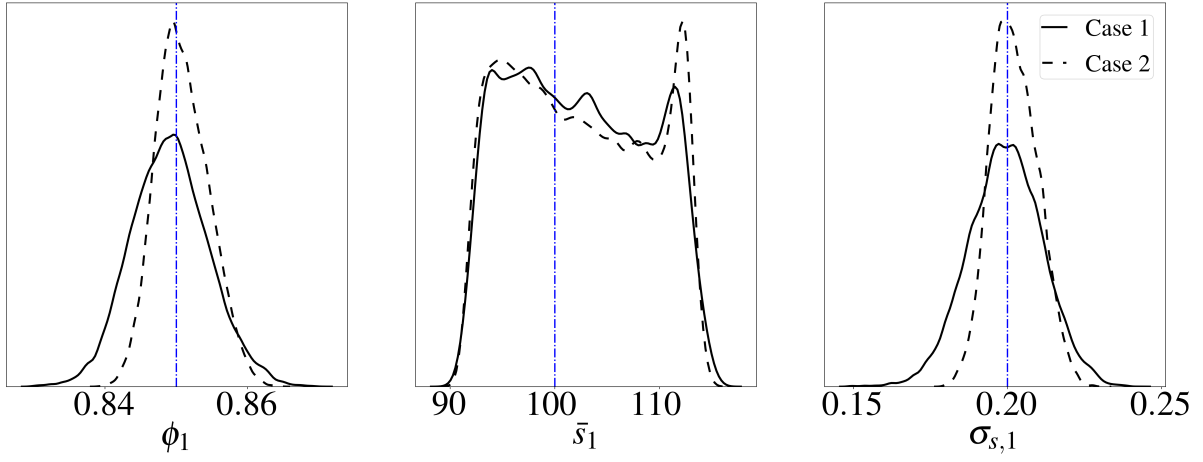


Figure 5: Posterior pdfs of the properties of material M_1 . The vertical line corresponds to the true value. ϕ is the porosity, \bar{s} is the mean pore size and σ_s is the normalized pore size standard deviation. The legend refers to Table 4.

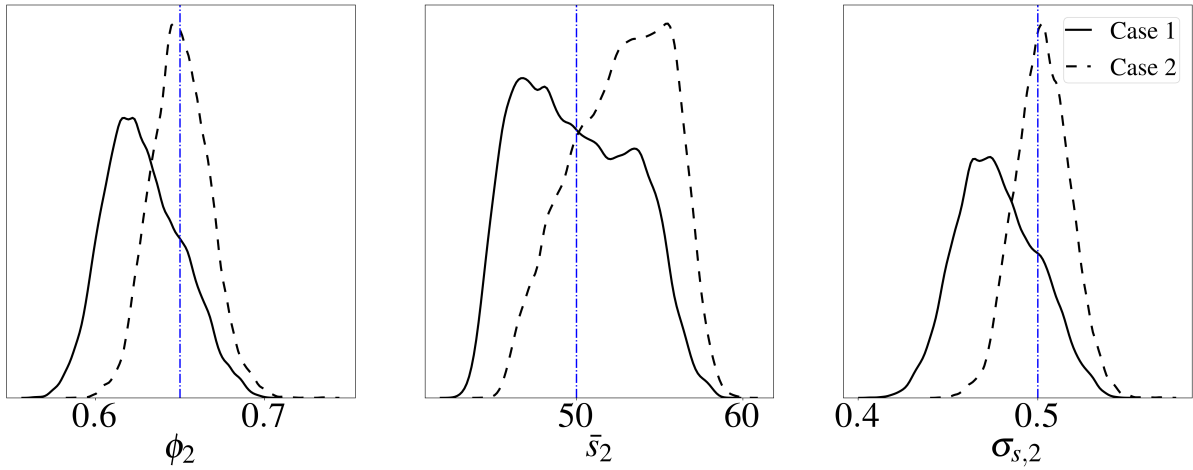


Figure 6: Posterior pdfs of the properties of material M_2 . The vertical line corresponds to the true value. ϕ is the porosity, \bar{s} is the mean pore size and σ_s is the normalized pore size standard deviation. The legend refers to Table 4.

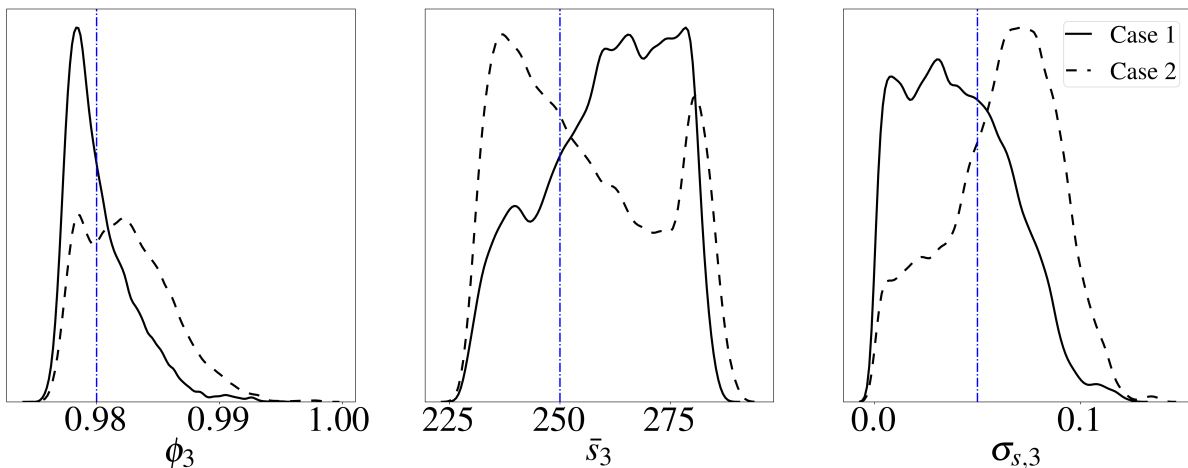


Figure 7: Posterior pdfs of the properties of material M_3 . The vertical line corresponds to the true value. ϕ is the porosity, \bar{s} is the mean pore size and σ_s is the normalized pore size standard deviation. The legend refers to Table 4.

It is observed that the Case 2 identification (with air gaps) yields better identification results for parameters ϕ and σ_s of materials M_1 and M_2 , when compared with Case 1 identification. Indeed, the posterior density is usually closer to the true value (vertical line) and has a narrower support. Since the pdfs are not normalized, a narrow support directly translates in the highest value of the pdf being higher than for broader pdfs. A narrower support means that more information was gained from the observed data.

We again remind the reader that both cases 1 and 2 have the same total number of observations. The only difference is that for Case 2, the observations are split between four different numerical experiments with $N_{\text{freq}} = 1200$, including three different air gaps, instead of just one numerical experiment with $N_{\text{freq}} = 4800$ with just the reference (no air gap) observation. If one were to keep $N_{\text{freq}} = 4800$ in Case 2 instead of down sampling the frequencies, the inference results (not displayed here for conciseness) would be pdfs that are narrower around the true values. However, there is a limit to what increasing N_{freq} will yield in terms of improved identification, and this limit, which is a function of the noise level, is not clearly understood.

For the identification of material M_3 , things are less clear cut, and the identification of the porosity is better in the reference case than it is with the addition of air gaps. Worse, a bimodality seems to appear in the pdf of the mean pore size \bar{s}_3 , signifying that ill-posedness (in the sense of non-uniqueness) starts to appear.

This identification test on single-layers is a first indication that diversifying the observation using air gaps could, in some cases, increase the information content available on the parameters to identify. This improvement might be material dependent, as in the case of material M_3 (see Fig. 7), where it seems slightly counterproductive to add “experiments” with additional air gaps. It is postulated that low resistivity materials (such as M_3) do no benefit as much from the addition of air gaps because of the air-cavity effect being less pronounced than for resistive materials. The different signals thus share a similar type of information content, and cannot be used as efficiently to improve one’s knowledge on the parameters.

In addition to the material properties, it is also important to check whether the other parameters have been well identified. Identification results of σ_R , σ_I , T , P and L are shown in Fig. 8 for material M_1 .

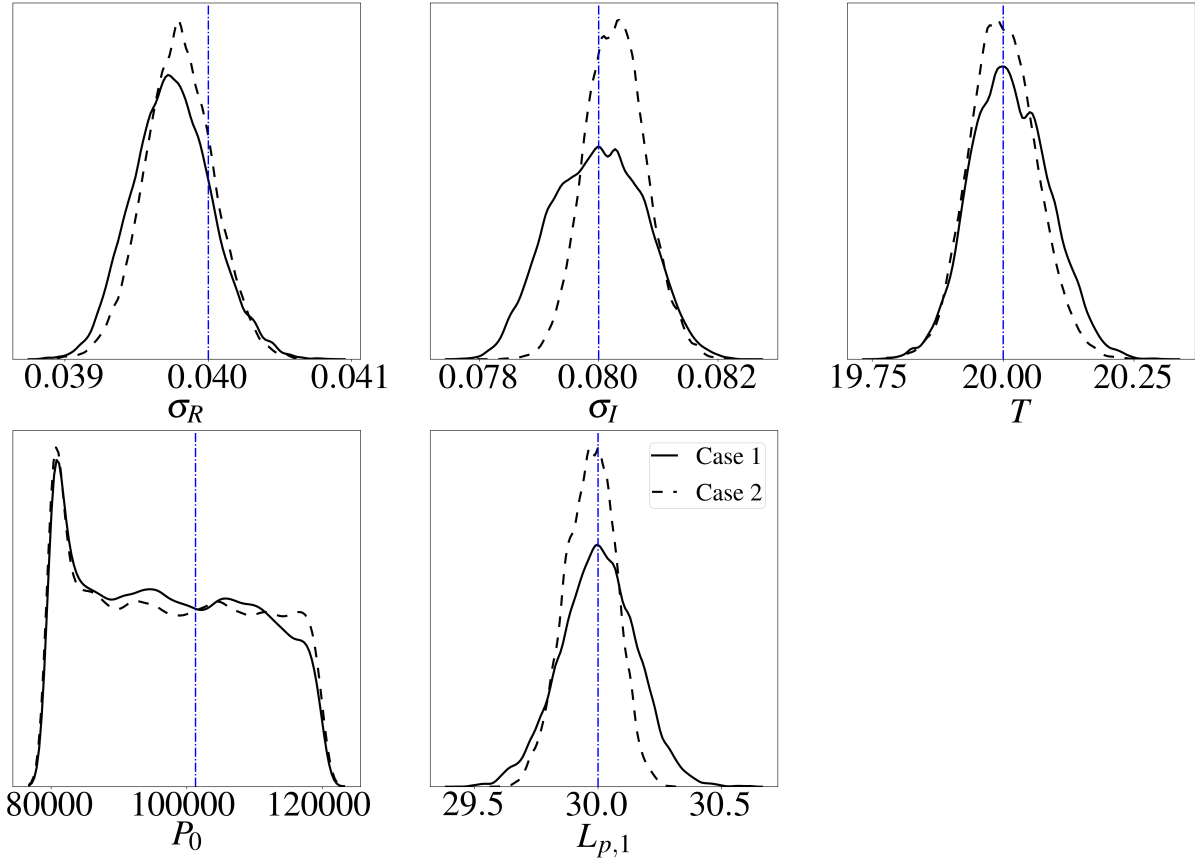


Figure 8: Posterior pdfs of the different parameters, during the identification of the properties of M_1 . The vertical line corresponds to the true value. σ_R (resp. σ_I) is the standard deviation of the real (resp. imaginary) part of the observed noisy pressure signals, T is the ambient temperature and P_0 the ambient pressure. $L_{p,1}$ is the sample thickness. The legend refers to Table 4.

All the parameters but the ambient pressure P_0 have been well estimated, with again a slight improvement in Case 2. Due to the low sensitivity of the ambient pressure, it was decided to reduce its range of variation in the prior model to within 5% of its nominal value (see Table 1), instead of 20% here, in order to facilitate the inference process. The density peak at low values of the ambient pressure remains unexplained, and was observed in all three identifications. It might be part of the reason why, in the presence of air gaps, a bi-modality appeared in the identification of M_3 .

As opposed to the ambient pressure, the temperature is a well identified parameter. This means that its influence on the education result is substantial. One could thus benefit from including the temperature as a parameter during the education process, instead of fixing its value at the measured one without accounting for uncertainties.

5.4 triple-layer identification

Qualitative identification results of the triple-layer porous materials are summarized in Figs. 9,10,11 in the form of posterior probability density functions.

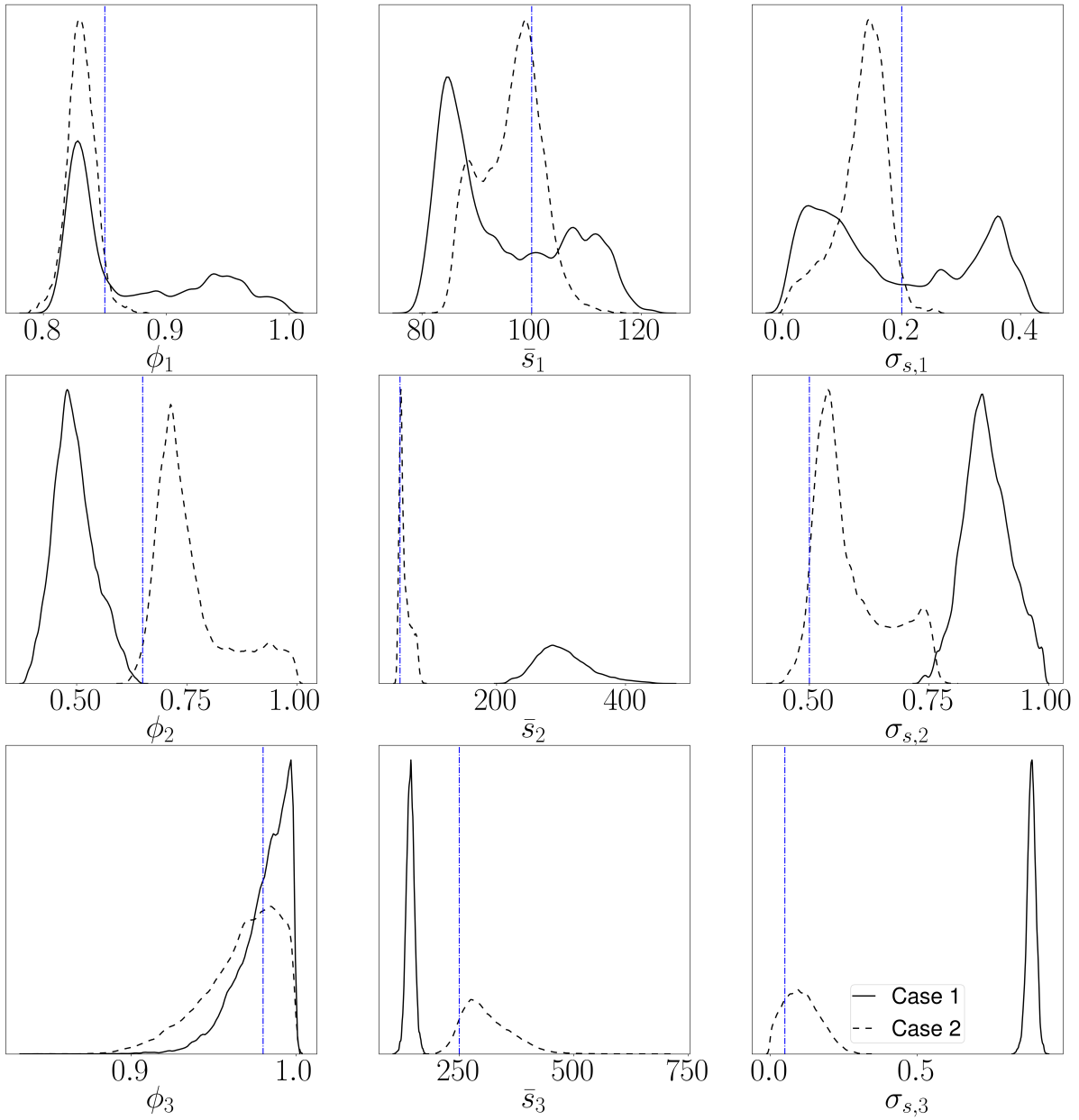


Figure 9: Posterior pdfs of the triple-layer $M_1 \circ M_2 \circ M_3$. The vertical line corresponds to the true value. The i^{th} layer has a porosity ϕ_i , a mean pore size \bar{s}_i and normalized pore size standard deviation $\sigma_{s,i}$. The legend refers to Table 4.

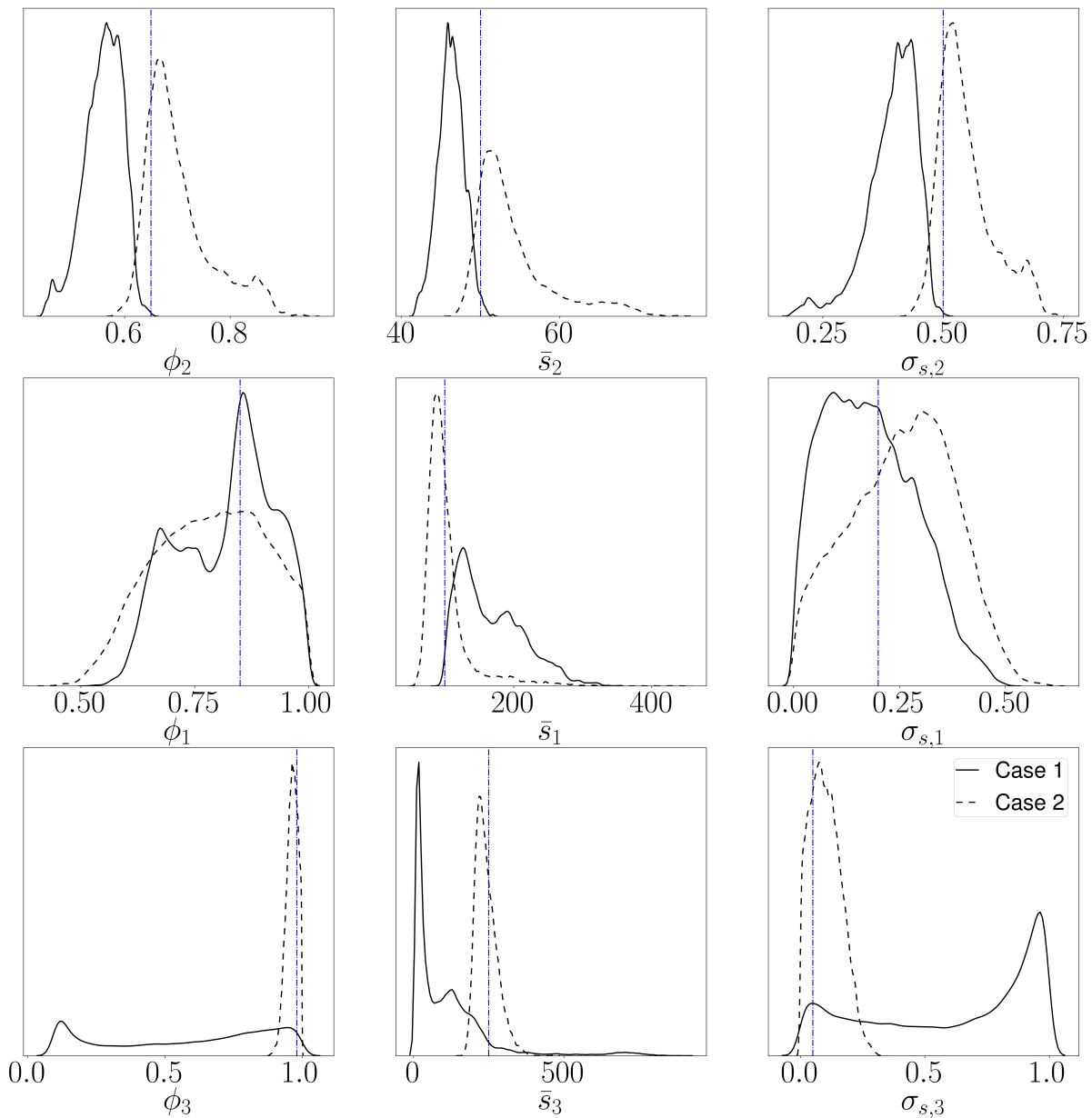


Figure 10: Posterior pdfs of the triple-layer $M_2 \circ M_1 \circ M_3$. The vertical line corresponds to the true value. The i^{th} layer has a porosity ϕ_i , a mean pore size \bar{s}_i and normalized pore size standard deviation $\sigma_{s,i}$. The legend refers to Table 4.

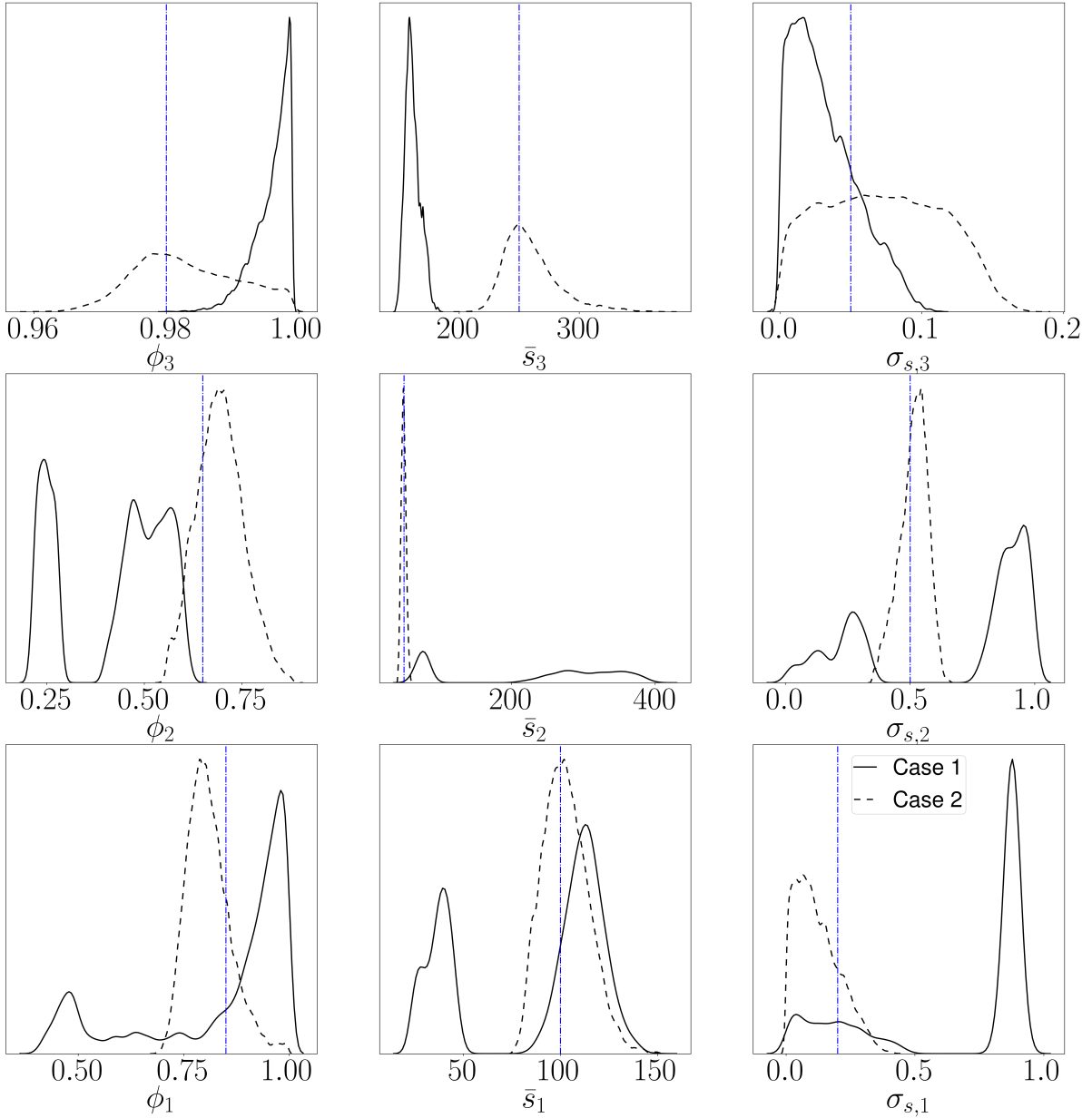


Figure 11: Posterior pdfs of the triple-layer $M_3 \circ M_2 \circ M_1$. The vertical line corresponds to the true value. The i^{th} layer has a porosity ϕ_i , a mean pore size \bar{s}_i and normalized pore size standard deviation $\sigma_{s,i}$. The legend refers to Table 4.

The reference method, Case 1, is first analyzed. When no air gap is considered during the inverse problem, the parameters of each layers are not always well identified.

For the identification of the triple-layer $M_1 \circ M_2 \circ M_3$ (Fig. 9), all 3 model properties of the second layer have been wrongly identified, and only the porosity was correctly found in the third layer. By wrongly identified, it is meant here that the support of the posterior pdf does not include the true value of the parameter. The properties of the first layer remain well identified.

This is most likely due to the signal being more sensitive to the first layer properties in impedance tubes. If the first layer does not let the waves through, then no information can be gained on the consecutive layers. We note the apparition of a bi-modal pdf for the model parameters of the first layer, in particular for the standard deviation of the pore size $\sigma_{s,1}$. This is a sign of non-uniqueness in the solution. Using a classical deterministic approach to inverse problem, each mode would correspond to a local minimum.

For the identifications of the remaining triple-layers (Figs. 10,11), the identification remains quite poor with the reference method (i.e., without air gaps). Wide posterior pdfs are obtained for the model parameters of the third layer of $M_2 \circ M_1 \circ M_3$ (Fig. 10), indicating that little information was gained via the observations (in particular for the porosity). The presence of bi-modal distributions is quite marked in Fig. 11, for the second and third layers of the sample, indicating again the appearance of a non-unique solution to the inverse problem.

Case 2 corresponds to the model parameter identification of each layer, when air gaps have been added behind the sample to artificially increase the number of observation. By reducing the amount of frequencies at which the signal is observed, the total amount of data remains the same between Case 1 and Case 2. Quite markedly, the identification with air gaps has drastically improved the solution of the inverse problems. In all the identifications that were performed (Figs. 9,10,11), all the material properties have been well identified (meaning that the true value falls within the posterior pdf). In addition, where there was a bi-modal pdf for certain parameters in the reference case, these are now gone. This means that the non-uniqueness of the problem has been removed.

Note that in Case 2, there are three additional parameters to identify (i.e., the air gaps lengths). As a result, the inference process is more difficult than for Case 1. Yet, identification results are improved.

To complement the discussion, the thickness parameters of each layer as well as the air gap lengths, are displayed for the identification of material $M_1 \circ M_2 \circ M_3$ in Fig. 12. Similar conclusions can be drawn, i.e., that the addition of air gaps has improved the identification, and removed the non uniqueness present in the thickness of the second and third layer of the material.

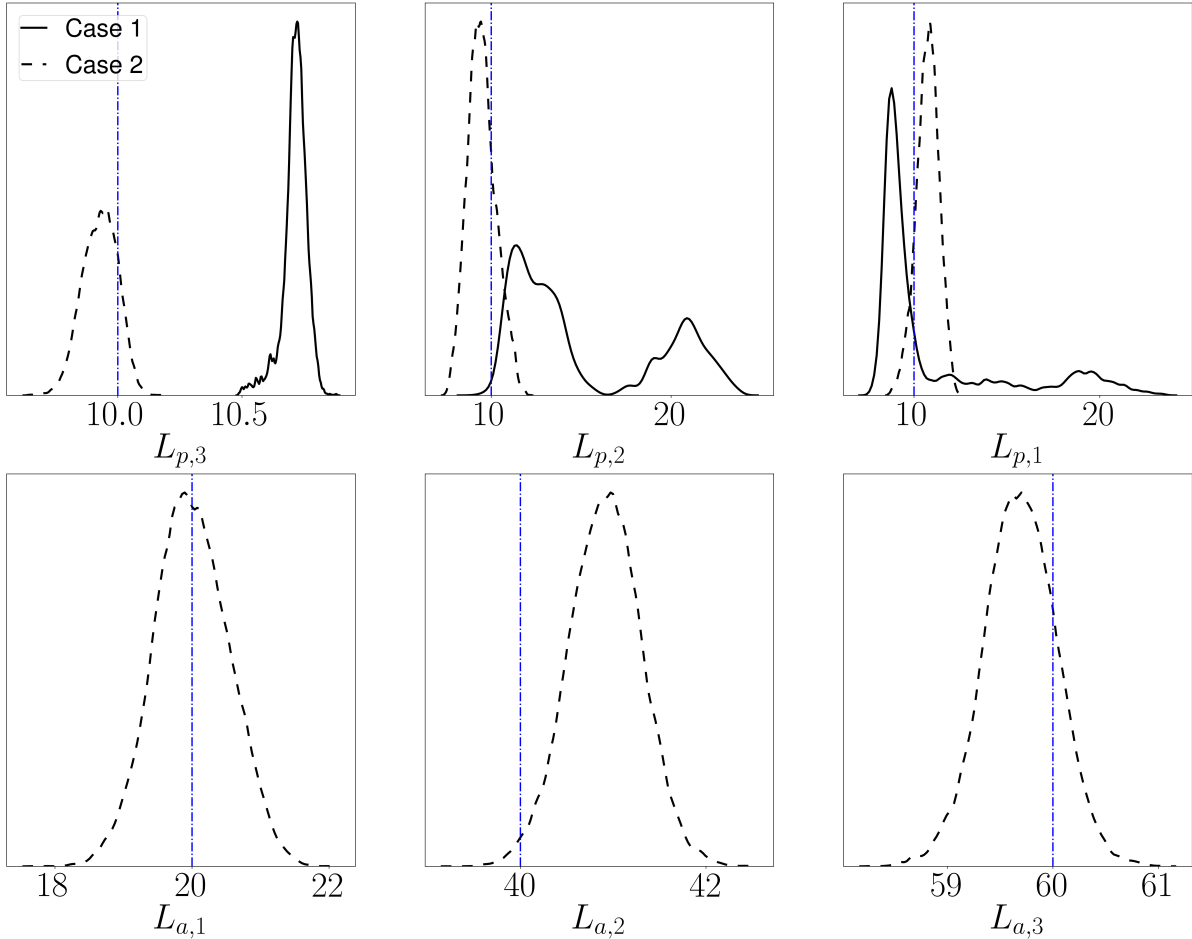


Figure 12: Posterior pdfs of the thickness of each layer of triple-layer $M_3 \circ M_2 \circ M_1$, and of the air gap lengths. The vertical line corresponds to the true value. The legend refers to Table 4.

5.5 Discussion

General comments on the previous material identifications are now highlighted.

The use of the Horoshenkov hypothesis in the JCAPL model is attractive for multi-layer identifications using impedance tubes, as an increase in the number of parameters would otherwise rapidly increase the difficulty of the inference. In addition, the JCAPL model is quite adapted to impedance tube studies, as it can be used in the intermediary frequency range, contrary to asymptotic models [27, 37].

An intrinsic limitation of the identification of multi-layer samples in impedance tubes is related to the fact that if a layer is placed behind another layer that is large or has a high resistivity, almost no wave is transmitted through it. As a result, the use of one or more air gaps would be

wasted, as the observation on the microphones of the impedance tube would remain the same.

It remains unclear how many air gaps are required to properly identify multi-layer materials. In additional tests, not presented here for conciseness, it was observed that even adding just one air gap could sometimes remove the non-uniqueness (bi-modality of the posterior pdf) in certain cases. The result is even more marked when all the frequency data is used. In the present work, the frequency data of the observed signals were down-sampled when air gaps were present, in order to keep the total amount of data the same between Cases 1 and 2, to focus on the influence of air gaps, relatively to the non-uniqueness.

For every air gap added to make a new observation, an additional parameter needs to be identified (the air gap length). It is then remarkable that despite having three additional parameters to identify, the cases with more air gaps systematically improve the identification results compared with the reference case. In practice, the experimenter could know quite precisely the thickness of each air gap, making it possible to restrain the support of the prior in Table 1. A similar constraint could be imposed on the total thickness of a multi-layer sample, which could further help removing the ill-posedness by forbidding unfeasible solutions.

When using a deterministic approach to inverse problems, by means of an optimization algorithm, one could directly apply this paper’s method using the log-likelihood as a cost function and the log-prior as a regularization parameter. Using multiple air gaps, the cost function becomes more regular, and gradient-descent algorithms could be used with less risks of ending in a local minimum that is not the global minimum.

When using high-frequency content time-domain signals, for instance with ultrasonic transducers, the present method needs to be adapted since an impedance tube cannot be used anymore. However, one could potentially add an air gap and a rigid plate behind the material to measure the total reflection coefficient of the combination, to cheaply obtain a second observation on the same material. This is akin to changing the angle of incidence of the ultrasonic wave, and using multiple measurements to identify material properties [23, 37]. Adding an air gap would also delay the arrival of the wave that was fully transmitted and then reflected on the rigid back-plate, back to the transducer, thus potentially allowing better wave decoupling in the time domain.

In practice, one often knows the length of each stacked material. However, if the materials are truly distinct, the identification of their properties would be simpler in the first place if measurements were done individually on each layer, and there would be no need to make the inference more difficult by considering multiple layers simultaneously. However, if the porous layers are not truly stiff, the vertical stacking of multiple layers could potentially change the pore geometry.

6 Conclusion

This paper was concerned with the numerical validation of a technique for the inverse identification of multi-layer rigid porous media in impedance tubes. The goal was to retrieve the model parameters (JCAPL-Horoshenkov) of each layer, assumed isotropic (1D propagation only).

Using the surface impedance or reflection coefficient signals as the input of an inverse problem for the identification of the intrinsic properties of porous media leads to biased results. This is caused by the unknown frequency dependence of the uncertainty on these signals, which are derived initially from microphone pressure measurements. A more efficient approach consists in directly using the pressure signals for the inverse problem input. When more than two microphones are used in the impedance tube, this approach then becomes strictly superior, as more information is gained.

A numerical analysis was conducted on 6 different materials, consisting in single-layer and triple-layer sample combinations. Using an objective Bayesian inference strategy, the model parameters pdf of each material configuration were retrieved. The inputs of the inference were synthetic noisy pressure signals evaluated at fictive microphone positions, mimicking an experiment inside an impedance tube.

In the reference identification case of triple-layer samples (no air gap), the model parameters were not properly identified: non-uniqueness was present in the solution, and the posterior pdf support remained very large. The strategy used in this work consisted in adding observations to feed the inference process, by the addition of air gaps behind the multi-layer samples. The frequency data was down-sampled when air gaps were considered, to keep equal the total amount of data used in the inference. It was shown that adding three different air gaps behind a triple-layer

sample almost systematically led to an improved identification for all the considered parameters. Adding the air gaps allowed the disambiguation in parameter estimation that was present in the reference case without air gap (non-uniqueness of the solution), and the posterior pdf support always included the true parameter value.

Acknowledgment

This work has been conducted under the ONERA-CNRS collaboration agreement on porous media acoustics. The authors would like to thank Estelle Piot for reviewing the early versions of this work.

Conflict of interest

The authors declare that they have no conflict of interest.

References

- [1] J. Allard, N. Atalla, Propagation of Sound in Porous Media: Modelling Sound Absorbing Materials 2e, John Wiley & Sons, New York, 2009. doi:10.1002/9780470747339.
- [2] J. M. Sabatier, H. E. Bass, L. N. Bolen, K. Attenborough, V. Sastry, The interaction of airborne sound with the porous ground: The theoretical formulation, The Journal of the Acoustical Society of America 79 (5) (1986) 1345–1352. arXiv:<https://doi.org/10.1121/1.393662>, doi:10.1121/1.393662.
URL <https://doi.org/10.1121/1.393662>
- [3] M. N. Toksoz, C. H. Cheng, A. Timur, Velocities of seismic waves in porous rocks, Geophysics 41 (4) (1976) 621–645.
- [4] T. Pointer, E. Liu, J. A. Hudson, Seismic wave propagation in cracked porous media, Geophysical Journal International 142 (1) (2000) 199–231. arXiv:<https://academic.oup>.

com/gji/article-pdf/142/1/199/1603864/142-1-199.pdf, doi:10.1046/j.1365-246x.2000.00157.x.

URL <https://doi.org/10.1046/j.1365-246x.2000.00157.x>

- [5] N. Xiang, J. M. Sabatier, Land mine detection measurements using acoustic-to-seismic coupling, in: A. C. Dubey, J. F. Harvey, J. T. Broach, R. E. Dugan (Eds.), *Detection and Remediation Technologies for Mines and Minelike Targets V*, Vol. 4038, International Society for Optics and Photonics, SPIE, 2000, pp. 645 – 655. doi:10.1117/12.396292.
URL <https://doi.org/10.1117/12.396292>
- [6] J. M. Sabatier, Ning Xiang, An investigation of acoustic-to-seismic coupling to detect buried antitank landmines, *IEEE Transactions on Geoscience and Remote Sensing* 39 (6) (2001) 1146–1154. doi:10.1109/36.927429.
- [7] A. Hosokawa, T. Otani, Ultrasonic wave propagation in bovine cancellous bone, *The Journal of the Acoustical Society of America* 101 (1) (1997) 558–562. doi:10.1121/1.418118.
- [8] S. Chaffai, F. Peyrin, S. Nuzzo, R. Porcher, G. Berger, P. Laugier, Ultrasonic characterization of human cancellous bone using transmission and backscatter measurements: relationships to density and microstructure, *Bone* 30 (1) (2002) 229–237. doi:10.1016/S8756-3282(01)00650-0.
- [9] Z. E. A. Fellah, J. Y. Chapelon, S. Berger, W. Lauriks, C. Depollier, Ultrasonic wave propagation in human cancellous bone: Application of biot theory, *The Journal of the Acoustical Society of America* 116 (1) (2004) 61–73. doi:10.1121/1.1755239.
- [10] T. Geyer, E. Sarradj, C. Fritzsche, Measurement of the noise generation at the trailing edge of porous airfoils, *Experiments in fluids* 48 (2) (2010) 291–308. doi:10.1007/s00348-009-0739-x.
- [11] J. Schulze, J. Sesterhenn, Optimal distribution of porous media to reduce trailing edge noise, *Computers & Fluids* 78 (2013) 41 – 53, IES of turbulence aeroacoustics and combustion.

doi:<https://doi.org/10.1016/j.compfluid.2011.12.022>.

URL <http://www.sciencedirect.com/science/article/pii/S004579301100394X>

- [12] M. Mößner, R. Radespiel, Flow simulations over porous media—comparisons with experiments, *Computers & Fluids* 154 (2017) 358–370. doi:10.1016/j.compfluid.2017.03.002.
- [13] Y.-B. Xiong, Y.-H. Zhu, P.-X. Jiang, Numerical simulation of transpiration cooling for sintered metal porous strut of the scramjet combustion chamber, *Heat Transfer Engineering* 35 (6-8) (2014) 721–729. arXiv:<https://doi.org/10.1080/01457632.2013.837790>, doi:10.1080/01457632.2013.837790.
URL <https://doi.org/10.1080/01457632.2013.837790>
- [14] G. Huang, Z. Min, L. Yang, P.-X. Jiang, M. Chyu, Transpiration cooling for additive manufactured porous plates with partition walls, *International Journal of Heat and Mass Transfer* 124 (2018) 1076 – 1087. doi:<https://doi.org/10.1016/j.ijheatmasstransfer.2018.03.110>.
URL <http://www.sciencedirect.com/science/article/pii/S0017931017355126>
- [15] W. Davern, Perforated facings backed with porous materials as sound absorbers-an experimental study, *Applied Acoustics* 10 (2) (1977) 85–112. doi:10.1016/0003-682X(77)90019-6.
- [16] M. Yang, P. Sheng, Sound absorption structures: From porous media to acoustic metamaterials, *Annual Review of Materials Research* 47 (2017) 83–114. doi:10.1146/annurev-matsci-070616-124032.
- [17] L. L. Beranek, Acoustic impedance of porous materials, *The Journal of the Acoustical Society of America* 13 (3) (1942) 248–260.
- [18] D. Bies, C. H. Hansen, Flow resistance information for acoustical design, *Applied Acoustics* 13 (5) (1980) 357–391. doi:10.1016/0003-682X(80)90002-X.
- [19] P. Leclaire, L. Kelders, W. Lauriks, M. Melon, N. Brown, B. Castagnede, Determination of the viscous and thermal characteristic lengths of plastic foams by ultrasonic measurements in helium and air, *J. App. Phys.* 80 (4) (1996) 2009–2012. doi:10.1063/1.363817.

- [20] R. Dragonetti, C. Ianniello, R. A. Romano, Measurement of the resistivity of porous materials with an alternating air-flow method, *The Journal of the Acoustical Society of America* 129 (2) (2011) 753–764. doi:10.1121/1.3523433.
- [21] P. Bonfiglio, F. Pompoli, Inversion problems for determining physical parameters of porous materials: Overview and comparison between different methods, *Acta Acustica united with Acustica* 99 (3) (2013) 341–351. doi:10.3813/AAA.918616.
- [22] K. V. Horoshenkov, A review of acoustical methods for porous material characterisation, *Int. J. Acoust. Vib* 22 (2017) 92–103. doi:10.20855/ijav.2017.22.1455.
- [23] L. De Ryck, W. Lauriks, P. Leclaire, J.-P. Groby, A. Wirgin, C. Depollier, Reconstruction of material properties profiles in one-dimensional macroscopically inhomogeneous rigid frame porous media in the frequency domain, *The Journal of the Acoustical Society of America* 124 (3) (2008) 1591–1606. doi:10.1121/1.2959734.
- [24] Z. A. Fellah, N. Sebaa, M. Fellah, F. Mitri, E. Ogam, C. Depollier, Ultrasonic characterization of air-saturated double-layered porous media in time domain, *Journal of Applied Physics* 108 (1) (2010) 014909. doi:10.1063/1.3456443.
- [25] C. J. Fackler, N. Xiang, K. V. Horoshenkov, Bayesian acoustic analysis of multilayer porous media, *The Journal of the Acoustical Society of America* 144 (6) (2018) 3582–3592. arXiv: <https://doi.org/10.1121/1.5083835>, doi:10.1121/1.5083835.
URL <https://doi.org/10.1121/1.5083835>
- [26] J.-D. Chazot, E. Zhang, J. Antoni, Acoustical and mechanical characterization of poroelastic materials using a bayesian approach, *J. Acoust. Soc. Am.* 131 (6) (2012) 4584–4595. doi:10.1121/1.3699236.
- [27] R. Roncen, Z. E. A. Fellah, D. Lafarge, E. Piot, F. Simon, E. Ogam, M. Fellah, C. Depollier, Acoustical modeling and bayesian inference for rigid porous media in the low-mid frequency regime, *The Journal of the Acoustical Society of America* 144 (6) (2018) 3084–3101. doi:10.1121/1.5080561.

- [28] R. Roncen, Z. Fellah, E. Piot, E. Ogam, Bayesian inference of a human bone and biomaterials using ultrasonic transmitted signals, *The Journal of the Acoustical Society of America* 146 (3) (2019) 1629–1640. doi:10.1121/1.5125263.
- [29] Y. Atalla, R. Panneton, Inverse acoustical characterization of open cell porous media using impedance tube measurements, *Canadian Acoustics* 33 (1) (2005) 11–24.
- [30] T. Hentati, L. Bouazizi, M. Taktak, H. Trabelsi, M. Haddar, Multi-levels inverse identification of physical parameters of porous materials, *J. Appl. Acoust.* (2015). doi:10.1016/j.apacoust.2015.09.013.
- [31] T. G. Zieliński, Normalized inverse characterization of sound absorbing rigid porous media, *J. Acoust. Soc. Am.* 137 (6) (2015) 3232–3243. doi:10.1121/1.4919806.
- [32] M. Niskanen, J.-P. Groby, A. Duclos, O. Dazel, J. Le Roux, N. Poulain, T. Huttunen, T. Lähivaara, Deterministic and statistical characterization of rigid frame porous materials from impedance tube measurements, *J. Acoust. Soc. Am.* 142 (4) (2017) 2407–2418. doi:10.1121/1.5008742.
- [33] Z. E. A. Fellah, S. Berger, W. Lauriks, C. Depollier, C. Aristegui, J.-Y. Chapelon, Measuring the porosity and the tortuosity of porous materials via reflected waves at oblique incidence, *J. Acoust. Soc. Am.* 113 (5) (2003) 2424–2433. doi:10.1121/1.1567275.
- [34] Z. E. A. Fellah, F. Mitri, C. Depollier, S. Berger, W. Lauriks, J. Chapelon, Characterization of porous materials with a rigid frame via reflected waves, *J. Appl. Acoust.* 94 (12) (2003) 7914–7922. doi:10.1063/1.1629386.
- [35] Z. E. A. Fellah, F. G. Mitri, M. Fellah, E. Ogam, C. Depollier, Ultrasonic characterization of porous absorbing materials: Inverse problem, *J. Sound. Vib.* 302 (4) (2007) 746–759. doi:10.1016/j.jsv.2006.12.007.
- [36] Z. E. A. Fellah, M. Sadouki, M. Fellah, F. Mitri, E. Ogam, C. Dépollier, Simultaneous determination of porosity, tortuosity, viscous and thermal characteristic lengths of rigid porous materials, *J. App. Phys.* 114 (20) (2013) 204902. doi:10.1063/1.4833546.

- [37] R. Roncen, Z. E. A. Fellah, F. Simon, E. Piot, M. Fellah, E. Ogam, C. Depollier, Bayesian inference for the ultrasonic characterization of rigid porous materials using reflected waves by the first interface, *The Journal of the Acoustical Society of America* 144 (1) (2018) 210–221. doi:10.1121/1.5044423.
- [38] R. Roncen, Z. Fellah, E. Piot, F. Simon, E. Ogam, M. Fellah, C. Depollier, Inverse identification of a higher order viscous parameter of rigid porous media in the high frequency domain, *The Journal of the Acoustical Society of America* 145 (3) (2019) 1629–1639. doi:10.1121/1.5095403.
- [39] M. Niskanen, O. Dazel, J.-P. Groby, A. Duclos, T. Lähivaara, Characterising poroelastic materials in the ultrasonic range—a bayesian approach, *Journal of Sound and Vibration* 456 (2019) 30–48. doi:10.1016/j.jsv.2019.05.026.
- [40] R. Roncen, Z. E. A. Fellah, E. Ogam, Bayesian inference of human bone sample properties using ultrasonic reflected signals, *The Journal of the Acoustical Society of America* 148 (6) (2020) 3797–3808. doi:10.1121/10.0002878.
- [41] Z. Lim, A. Putra, M. Nor, M. Yaakob, Sound absorption performance of natural kenaf fibres, *Applied Acoustics* 130 (2018) 107 – 114. doi:https://doi.org/10.1016/j.apacoust.2017.09.012.
URL <http://www.sciencedirect.com/science/article/pii/S0003682X17305583>
- [42] N. Sellen, M.-A. Galland, O. Hilbrunner, Identification of the characteristic parameters of porous media using active control, in: 8th AIAA/CEAS Aeroacoustics Conference, Breckenridge, Colorado, 2002. doi:https://doi.org/10.2514/6.2002-2504.
- [43] D. L. Johnson, J. Koplik, R. Dashen, Theory of dynamic permeability and tortuosity in fluid-saturated porous media, *J. Fluid Mech.* 176 (1987) 379–402. doi:10.1017/S0022112087000727.
- [44] Y. Champoux, J.-F. Allard, Dynamic tortuosity and bulk modulus in air-saturated porous media, *J. Appl. Acoust.* 70 (4) (1991) 1975–1979. doi:10.1063/1.349482.

- [45] S. R. Pride, F. D. Morgan, A. F. Gangi, Drag forces of porous-medium acoustics, *Phys. Rev. B* 47 (9) (1993) 4964–4978. doi:10.1103/PhysRevB.47.4964.
- [46] D. Lafarge, P. Lemarinier, J. F. Allard, V. Tarnow, Dynamic compressibility of air in porous structures at audible frequencies, *J. Acoust. Soc. Am.* 102 (4) (1997) 1995–2006. doi:10.1121/1.419690.
- [47] K. V. Horoshenkov, A. Hurrell, J.-P. Groby, A three-parameter analytical model for the acoustical properties of porous media, *The Journal of the Acoustical Society of America* 145 (4) (2019) 2512–2517. doi:10.1121/1.5098778.
- [48] M. Åbom, H. Bodén, Error analysis of two-microphone measurements in ducts with flow, *The journal of the acoustical society of America* 83 (6) (1988) 2429–2438. doi:10.1121/1.396322.
- [49] R. C. Smith, *Uncertainty quantification: theory, implementation, and applications*, Vol. 12, Siam, Philadelphia, 2013.
- [50] C. J. ter Braak, J. A. Vrugt, Differential evolution markov chain with snooker updater and fewer chains, *Statistics and Computing* 18 (4) (2008) 435–446. doi:10.1007/s11222-008-9104-9.
- [51] J. A. Vrugt, C. Ter Braak, C. Diks, B. A. Robinson, J. M. Hyman, D. Higdon, Accelerating markov chain monte carlo simulation by differential evolution with self-adaptive randomized subspace sampling, *International Journal of Nonlinear Sciences and Numerical Simulation* 10 (3) (2009) 273–290.
URL <https://www.osti.gov/biblio/960766>
- [52] E. Laloy, J. A. Vrugt, High-dimensional posterior exploration of hydrologic models using multiple-try DREAM(ZS) and high-performance computing, *Water Resour. Res.* 48 (2012) W01526. doi:10.1029/2011WR010608.
- [53] A. Gelman, D. B. Rubin, Inference from iterative simulation using multiple sequences, *Statistical science* 7 (4) (1992) 457–472. doi:10.1214/ss/1177011136.

- [54] E. M. Shockley, J. A. Vrugt, C. F. Lopez, PyDREAM: high-dimensional parameter inference for biological models in python, *Bioinformatics* 34 (4) (2017) 695–697. arXiv:<https://academic.oup.com/bioinformatics/article-pdf/34/4/695/25117213/btx626.pdf>, doi: 10.1093/bioinformatics/btx626.
URL <https://doi.org/10.1093/bioinformatics/btx626>
- [55] A. Wirgin, The inverse crime, arXiv preprint math-ph/0401050 (2004).
- [56] M. Waskom, O. Botvinnik, D. O’Kane, P. Hobson, S. Lukauskas, D. C. Gemperline, T. Augspurger, Y. Halchenko, J. B. Cole, J. Warmenhoven, J. de Ruiter, C. Pye, S. Hoyer, J. Vanderplas, S. Villalba, G. Kunter, E. Quintero, P. Bachant, M. Martin, K. Meyer, A. Miles, Y. Ram, T. Yarkoni, M. L. Williams, C. Evans, C. Fitzgerald, Brian, C. Fonnesbeck, A. Lee, A. Qalieh, mwaskom/seaborn: v0.8.1 (september 2017) (Sep. 2017). doi: 10.5281/zenodo.883859.
URL <https://doi.org/10.5281/zenodo.883859>